Behaviour of liquid droplets bouncing onto a hot slab

F. Lelong[1*], M. Gradeck[2], N. Seiler[1], P. Ruyer[1], G. Castanet[2] and P. Dunand[2]
[1]IRSN/DPAM, Cadarache Bâtiment 700, BP3 13 115 Saint Paul lez Durance cedex,
[2]LEMTA Nancy-University CNRS, 2 avenue de la forêt de Haye, BP160 2057 54504 Vandoeuvre cedex

Abstract

The rebound of a liquid droplet stream impinging a hot surface ($T_W = 500 - 600^o$C) in the Leidenfrost regime and the associated heat exchanges have been experimentally studied. In this particular impact regime, a thin vapour layer appears between the droplets and the overheated slab so that direct contact with the hot solid is avoided. For low Weber number, the surface energy is high enough compared to the kinetic energy to permit the rebound of the droplet which recovers its initial shape without breaking up. The generated vapour layer thermally insulates the droplet and minimizes the loss of heat from the surface at the impact. In this paper, an analytical approach is proposed for the modelling of the heat transfer between the drop and the heated wall. This model is based on combined dynamical and thermal considerations. On the one hand, the droplet dynamics is considered through a spring analogy in order to evaluate the evolution of droplet features such as the spreading diameter and the resident time when the droplet is squeezed above the hot surface. On the other hand, thermal parameters, such as the thickness of the vapour cushion beneath the droplet, are determined from an energy balance. Finally, the results are compared to experimental data.

Introduction

In a pressurized water reactor (PWR), during a Loss Of Coolant Accident (LOCA), the fuel assemblies are not cooled anymore by the surrounding liquid water; the temperature rises to such an extent that some parts of the fuel assemblies can be deformed resulting in 'ballooned regions' (Figure 1). When reflooding occurs, the cooling of these partially blocked parts of the fuel assemblies will depend on the coolant flow characteristics including overheated vapour and undersaturated droplets. So far, most of the existing models for heat transfers focused on the cooling of ballooned regions by vapor convection [1] [2]. However a two-phase mist flow is created during this process (*i.e.* a post dry-out dispersed flow regime) and the possibility of additional cooling by direct liquid droplet impingement on the blockage surfaces cannot be ignored. Because this topic is crucial for the safety of PWR reactor, the French 'Institut de Radioprotection et de Sûreté Nucléaire' (IRSN) carries out studies on the coolability of ballonned regions in the frame of its research program on Nuclear Fuel Safety.

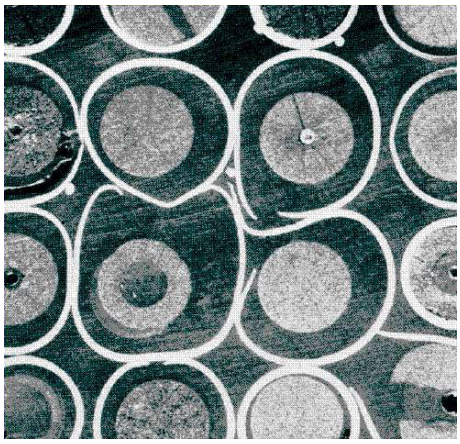

Figure 1. View of a real ballonned zone from the experiment PHEBUS LOCA-vertical cut of 16 fuel rods and their swollen cladding.

Preliminary studies about LOCA [3] reveal that the droplet diameters are expected to be in the range of $50\mu m$ - $1mm$, and their velocity in the range of $1-30m/s$, while the wall temperature is above 600^{o}C which is much hotter than the Leidenfrost temperature of liquid water even at the estimated ambient pressure. Under such conditions,

*Corresponding author: franck.lelong@irsn.fr

the impact regimes are predominantly the bouncing and the splashing regimes, depending on the droplets velocity and mass. Since the expected wall temperature is well above the Leidenfrost temperature [4], droplets are unable to wet the wall surface. A thin vapour layer actually remains between each droplet and the wall.

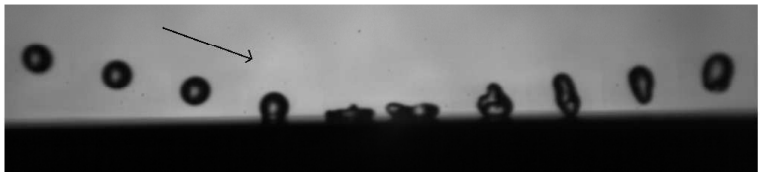

Figure 2. $300\mu m$ droplet stream impinging onto the slab ($T_w = 450^oC$, $V_n = 2m/s$)

Wachters [5] was certainly the first to study the impact of water droplets impinging on a horizontal surface heated at 400^{o}C. The outcomes of the impact were classified into three general categories depending on the droplet Weber number. For $We\ (= \frac{\rho_L D_d V^2}{\sigma}) < 30$, the droplet perfectly rebounds. For intermediate Weber numbers ($30 < We < 80$), the droplet splits into a large droplet and small satellite droplets. Finally for $We > 80$, the droplet breaks into several small droplets. In LOCA conditions, the Weber number is expected to be less than 50 what implies that the observed impact regime is the perfect bouncing one.

Even if many experimental studies concerning the dynamics of droplets impacting onto a heated surface are extensively reported in the literature (e.g. [6]), very few studies focus on the heat exchange between each droplet and the wall in the bouncing regime. Kendall [7] however assumed that only a part of the droplet evaporates; the heat flux removed from the wall by the contact of the droplet was derived on the basis of the heat exchange effectiveness (say ϵ). This quantity is the ratio of the exchanged energy during the bounce which is assumed to lead to evaporation of a part of the droplet (E_{DC}) to the energy required to evaporate its whole mass ($m_d L_{LV}$). According to the authors, its value lies in the range of 0.001 and 0.003. Ueda [8] found higher values for lower slab temperatures: the effectiveness belonging to $0.005 - 0.007$ under a wide range of conditions.

Latter, Guo [9] derived a mechanistic modelling for this direct droplet contact heat exchange. He also considered that the whole heat removed from the wall lead to the evaporation of a part of the droplet and wrote that this time averaged heat transfer is an integral over the droplet resident time on the wall (t_R defined as the duration between the impingement time where the droplet starts to squeeze and the time when the droplet is leaving the wall region), of the conductive heat flux between the flattened surface in front of the heated wall (called the base) (assumed at $T = T_{SAT}$) and the wall (at $T = T_W$) through a constant vapour layer of thickness δ_V :

$$E_{DC} = \int_0^{t_R} \frac{\lambda_V S_d(t)(T_W - T_{SAT})}{\delta_V} dt \tag{1}$$

where $S_d(t)$ is the droplet base surface, depending on the spreading diameter $D_s(t)$ of the droplet which is expressed, based on experimental results, at time t as :

$$\big(D_s(t)/D_d\big)^2 = 6.97\left[\frac{t}{t_R} - (\frac{t}{t_R})^2\right] \tag{2}$$

where D_d is the initial droplet diameter. The vapour layer thickness (δ_v) is controlled by the balance between the acceleration of the droplet in the normal direction to the wall and the recoil force generated due to the strong evaporation at its base.

Biance [10] derived correlations for the resident time based on the Rayleigh's theory and for the maximum spreading diameter from experimental results.

$$t_R = 2.65\sqrt{\frac{\rho_L D_d^3}{8\sigma}} \qquad\qquad D_{s,max}/D_d = We^{0.25} \tag{3}$$

These latter expressions were derived in the case of free falling droplets and their assessment for different injection velocities has not been carried out yet. Moreover, the resident time and the spreading diameter were not correlated to the droplet/wall heat exchange.

The present work, achieved in collaboration between LEMTA and IRSN, aims at accurately characterizing this heat flux. As the interaction between the droplets and the wall is very fast (a fraction of ms for the droplet size of

interest) and the heat fluxes very small (a few mW), an experimental set-up to measure the transfered heat during the resident time has been accurately designed and a specific inverse conduction measurement technique has been elaborated [11]. The experiments in room air are performed with very small droplets (about 80-300μm) injected at high frequency using a purpose-designed piezoelectric that allows to adjust the droplet frequency, velocity, size at the injection. The wall is a very thin disk of Nickel (250 to 500μm thickness) heated beforehand around 600^{o}C by an electromagnetic inductor. At initial time, heating is shut down and the heat flux removed from the wall by the impinging droplets (front face of the disk) is deduced by coupling the temperature field (measured in the rear face of the disk using an infrared camera) to the developed semi-analytical inverse heat conduction model. A high-speed camera is used to visualize the impingement process. The images are processed in order to determine the droplet incident angle and velocity, as well as its resident time and spreading diameter. The kinetic parameters, *i.e.* the droplet normal velocity and diameter, have a strong influence on the spreading diameter and on the resident time. An increase of the Weber number via these parameters induces the rise of the spreading diameter and of the resident time and, consequently, a rise of the droplet/wall heat exchange [12] and of the droplet heating rate [13].

In the following, we propose an analytical approach for the modelling of the heat transfer between the drop and the heated wall during a bounce. This model involves combined dynamical and thermal approaches. Finally, the results are compared to the Guo's correlation and to experimental data.

Theoretical analysis

To derive the droplet contact heat transfer model, we consider the impact of a single droplet bouncing onto the hot wall.

The droplet first flattens out on the thin vapour layer that forms beneath the droplet leading to the thermal insulation of the liquid from the hot wall (because the wall temperature is well above the Leidenfrost temperature; about 220 ^oC for sessile water droplets placed on a Nickel flat surface). Then the droplet recovers its spherical shape after leaving the wall because surface tension overcomes inertia. The surface of droplet in front of the hot wall continuously varies during the impact. It is assumed that it forms a disk charaterized by the spreading diameter ($D_s(t)$) (see figure 3).

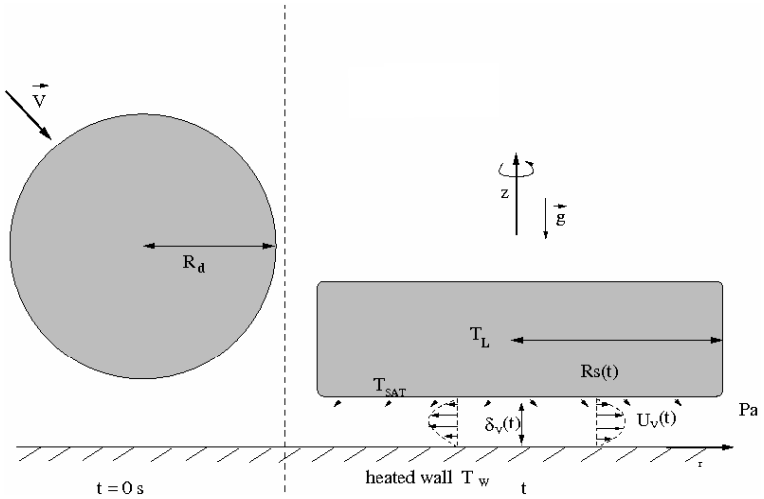

Figure 3. Schematic view of the droplet deformation.

During this bounce, heat is exchanged through the vapour layer. One considers that the heat removal (Φ [J]) from the wall at temperature T_W due to presence of the droplet at T_L (above a $\delta_V(t)$ thickness of vapour at T_V) is the sum of convective and radiative heat fluxes :

$$\Phi = \int_0^{t_R} Nu \frac{\lambda_V}{\delta_{V,1}(t)} (T_W - T_V) \pi R_s^2(t) dt + \int_0^{t_R} \epsilon_w \sigma_B (T_W^4 - T_L^4) \pi R_s^2(t) dt \quad (4)$$

where ϵ_w is the wall surface emissivity and σ_B the Stephan-Boltzmann's constant. The convective heat flux is expressed from a Nusselt number combined with a conductive heat transfer between the wall and the vapour through the $\delta_{V,1}(t)$ vapour thickness ($\delta_{V,1}(t) < \delta_V(t)$ in figure 3) which is itself controlled by the vapour production beneath the droplet.

To solve equation 4, some unknown variables should be expressed : the spreading diameter, the resident time and the vapour cushion thickness.

As shown by various authors [7], [8], [9], [15], only a very small part of the droplet evaporates during its rebound (less than 1%). Thus the droplet volume is kept constant during the bounce and both dynamical and thermal approaches could be considered separately. The dynamical approach concerns the droplet bounce focussed on its base spreading. And in the thermal approach, only the vapour flow in the interlayer is considered, the droplet base spreading being a boundary condition.

Spring analogy

In an attempt to describe the dynamic behaviour of the droplet, it is assimilated to a spring as proposed by Biance [10]. The droplet deformation over the vapour cuhsion induces a recoiling force that tends to make the droplet to return to its initial spherical shape. In the proposed spring analogy, as a crude simplification, the liquid mass is split into two point masses, located at the top and bottom locations of the spring. The equivalent stiffness k is linked to the surface tension and the damping coefficient η to the viscous energy dissipation (figure 4). The equation of motion of the spring-mass system is written within the frame of reference where Y=0 corresponds to the wall surface. During all the contact time of interest, m_2 is located on the liquid/vapour interface and $Y_2 = 0$.

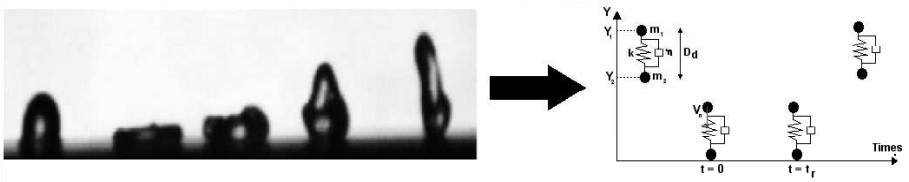

Figure 4. Representation of the spring analogy- V_n normal impact velocity; t_R resident time

The droplet deformation is charaterized by the displacement of the upper point mass (said m_1 in figure 4). The spring impacts the slab with an initial kinetic energy. The upper mass has, at t=0s, a normal velocity V_n which will set the system in motion. The Newton's equation applied to the m_1 mass (eq. 5) is :

$$m_1 \frac{d^2 Y_1}{dt^2} + \eta \frac{dY_1}{dt} + k(Y_1 - D_d) = -m_1 g \tag{5}$$

With the following boundary conditions, $Y_1(t=0) = D_d$ and $\frac{dY_1}{dt}(t=0) = V_n$, and introducing the system eigen pulsation ($\omega_0^2 = k/m_1$), it yields for a sub critical damping :

$$Y_1(t) = \frac{g}{\omega_0^2} e^{-\lambda t} \Big[cos(\omega_1 t) - \frac{\omega_0}{\omega_1} (2\pi r_t + r_d) sin(\omega_1 t) \Big] - \frac{g}{\omega_0^2} + D_d \tag{6}$$

with the variable $\lambda = \eta/(2\ r\ m_d)$, r being the droplet mass repartition ratio which is arbitrary taken to 0.5, $\omega_1 = \sqrt{\omega_0^2 - \lambda^2}$ is the eigen pulsation of the sub critical regime, $r_d = \lambda/\omega_0$ the damping factor , $r_t = t_{lim}/t_0$ with $t_0 = 2\pi/\omega_0$ the droplet oscillation period and $t_{lim} = V_n/g$. As the droplet undergoes a rebound without a noticeable loss of liquid by evaporation and neglecting the thermal expansion due to the liquid heating, the volume conservation can be written considering that a spherical droplet is distorted towards an oblate spheroid of height $Y_1(t)$:

$$4/3\pi R_d^3 = 2/3\pi R_s(t)^2 Y_1(t) \tag{7}$$

Combining equations 6 and 7, it comes :

$$R_s(t) = (2R_d^3)^{1/2} \Big(\frac{g}{\omega_0^2} e^{-\lambda t} \Big[cos(\omega_1 t) - \frac{\omega_0}{\omega_1} (2\pi r_t + r_d) sin(\omega_1 t) \Big] - \frac{g}{\omega_0^2} + D_d \Big)^{-1/2} \tag{8}$$

The equivalent stiffness k is evaluated thanks to an analogy between the supplied energy when the spring is deformed and the surface energy related to the surface tension during the change in shape of the droplet. Doing that, results reveal that the equivalent stiffness is not constant and highly nonlinear with respect to the droplet deformation (say Def in figure 5). For the sake of simplicity, a constant equivalent stiffness is determined considering the average between the maximum and minimum stiffnesses. The minimum stiffness is obtained for a tiny droplet

deformation whereas the maximum one is reached for the larger deformation when all the droplet kinetic energy has been converted into surface energy if the damping is nil. The equivalent stiffness is thus given by equation 9 where it depends not only on the surface tension but on the initial droplet kinetic energy.

$$k = \Big[\frac{2\pi}{5} + \frac{\pi We}{24\big(\frac{6}{12+We} - 1\big)^2}\Big]\sigma \tag{9}$$

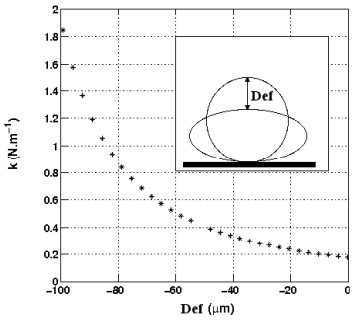

Figure 5. Equivalent stiffness, $D_d = 140\mu m$, $V_n = 4m/s$

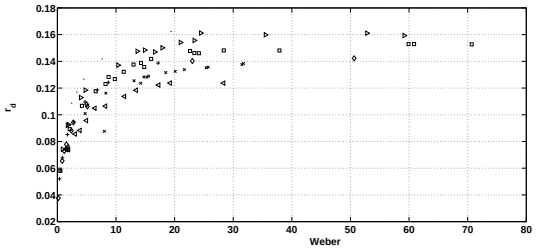

Figure 6. r_d variable versus the Weber number

The damping coefficient η is assimilated, in the spring analogy, to the viscous dissipation in the droplet internal flow generated by its deformation. From a dimensional analysis, it yields :

$$\eta = J\mu_L D_d Re^j \tag{10}$$

with the constants set (J;j=0.23;0.9) being determined from two experimental results, one for small and the second for large Weber numbers.

The $r_d = \lambda/\omega_0$ values calculated in our experimental conditions (Water ($\times$), Acetone ($\triangleright$), Ethanol ($\square$), Heptane ($\lozenge$), Hexanol ($\bullet$), Isoprophyl alcohol ($\triangleleft$), Decane (+)) are displayed in figure 6 attesting the assumption of a sub critical damping ($r_d < 1$).

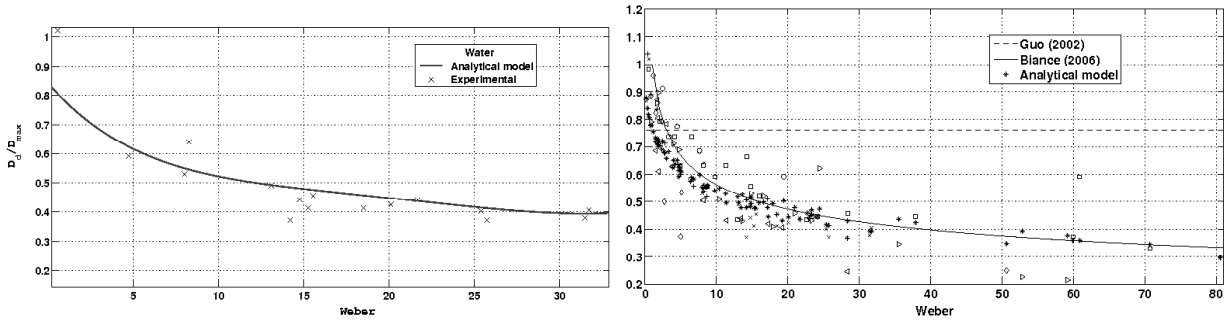

Figure 7. Maximum spread diameter evolution versus the Weber number for various fluids

The model gathering equations 8 - 10 has been compared to data for various Weber numbers and different fluids (Water ($\times$), Acetone ($\triangleright$), Ethanol ($\square$), Heptane ($\lozenge$), Hexanol ($\bullet$), Isoprophyl alcohol ($\triangleleft$), Decane (+)). The Guo's droplet base diameter (eq. 2) and Biance's spreading diameter (3b) have also been plotted in the same figure 7.

The present and the Biance's models well match all the data whereas the Guo's diameter remains constant. However, on the contrary to the Biance's model which is based on experimental results, the developed model is analytical and presents two advantages for the heat flux modelling : it gives the spreading diameter evolution and not only the maximum diameter and it takes into account the fluid properties and gives satisfactory results whatever the fluid is.

Furthermore, the resolution of heat exchange (4) requires the knowledge of the resident time of the droplet on the slab. This variable could be derived from the same spring analogy. It corresponds to the time where the

mass m_2 takes off considering a force balance. However, the Biance's correlation (3a) has been chosen for sake of simplicity because its result well matches our data [12].

Finally, the dynamical approach of this problem allows to get $R_s(t)$ and t_R, while the thermal approach will provide an estimate of $\delta_V(t)$.

Thermal balance

As a droplet gets closer to the hot wall, it experiences a recoil force generated by the liquid evaporation at the droplet base and an excessive pressure inside the thin vapour layer. The schetch of the droplet modelled as a liquid disk is displayed in figure 3.

The vapour thickness is the outcome of the equilibrium between the inertia of the droplet and this recoil force which comes from the liquid evaporation. Considering the vapour flow within the interlayer, the vapour velocity normal to the wall is neglected. Indeed, the vapour film is very thin (few tens of μm) compared to the base surface. Thus the vapour velocity is only radial. Assuming that this vapour flow is laminar, it yields :

$$\begin{cases} \mu_V \dfrac{\partial^2 u_V}{\partial z^2} = \dfrac{\partial P}{\partial r} \\ \dfrac{\partial P}{\partial z} = 0 \end{cases} \tag{11}$$

Considering the no-slip boundary conditions at both the wall and the liquid/vapour interface, equation 11 can be integrated to obtain the expression of $u_V(z,r)$ as a function of the radial pressure gradient. The vapour source intensity is obtained assuming that all the heat transfer to the interface is spent on evaporation. The vapour mass flow rate ($G[kg/m^2/s]$) is assumed to be uniformly generated beneath the droplet. The conservation of the mass flow rate leads to a relationship between G and the vapour velocity (12) and thus to the radial pressure gradient.

This pressure gradient is integrated over the radial direction with the atmospheric pressure (Pa) as boundary condition outside the vapour interlayer ($r = R_s(t)$) (eq. 12b).

$$\pi R_s(t)^2 G = \int_0^{\delta_V} 2\pi\rho_V R_s(t) u_V dz \qquad\qquad P_V(r,t) - Pa = \frac{3\mu_V G}{\delta_V^3(t)\rho_V}[R_s^2(t) - r^2] \tag{12}$$

This pressure difference is also obtained through the expression of the recoil force from a second Netwon's law projected on axis z :

$$\int_0^{R_s(t)} [P_V(r,t) - Pa] 2\pi r dr = \rho_L \frac{4}{3}\pi R_d^3 (g + a_n) \tag{13}$$

where g is the gravity acceleration and a_n the initial normal acceleration to the wall of the droplet expressed as $V_n/(t_R/2)$.

Combining equations 12b and 13, one gets :

$$\frac{3\mu_V G\pi R_s^4(t)}{2\delta_V^3(t)\rho_V} = \rho_L \frac{4}{3}\pi R_d^3 (g + a_n) \tag{14}$$

that relates the equilibrium between the droplet inertia and the recoil force.

Finally to express G, assumption is made that only the heat transfered by convection between the heated vapour and the liquid/droplet interface is absorbed by the droplets. Indeed, only a very little part of the radiative heat is absorbed by the droplet. The spectral absorption coefficient of one droplet of diameter between 100 and 300 μm, for wavelengths over 4 μm ($T_W < 500^oC$), obtained using the Mie theory, is about $10^{-7}m^{-1}$. And the covered distance of the ray inside the droplet is no more than about some hundred of μm.

The convective heat form vapour to droplet interface (at T_{SAT}) is expressed from a Nusselt number combined with a conductive heat transfer through a $\delta_{V,2}(t)$ vapour thickness (such as $\delta_V(t) = \delta_{V,1}(t) + \delta_{V,2}(t)$). Doing an energy balance on the liquid/vapour interface, it comes that this convective heat leads to, on the one hand the heating of a mass of liquid from T_L to T_{SAT} and on the second hand its evaporation.

Equation 15 gives the expression of G.

$$G = \frac{Nu\ \lambda_V (T_V - T_{SAT})}{\delta_{V,2}(t) h_{LV}^*} \tag{15}$$

with h_{LV}^* an enthalpy difference : $h_{LV}^* = h_{LV} + C_{p_L}(T_{SAT} - T_L)$.

Finally, combining equations 14 and 15 and assuming a linear variation of the vapour temperature through the thickness $\delta_V(t)$ such as for $\delta_{V,1}(t) = \delta_{V,2}(t)$, $T_V = (T_W + T_{SAT})/2$, the following equation is found for δ_V :

$$\delta_V(t) = \Big[\frac{9}{4}\frac{\mu_V R_d Nu\ \lambda_V (T_V - T_{SAT})}{\rho_V h^*_{LV} \rho_L [a_n + g]}\Big]^{1/4} \frac{R_s(t)}{R_d} \tag{16}$$

with $Nu = 5.39$ corresponding to the case of forced convection in a fully-developped laminar confined flow between an uniform heated surface and an insulated surface [16]. Indeed, average vapour velocity ($\bar{u}_V$) is obtained from integrations over the vapour thickness and the spreading radius. According to this analytical evaluation, the related values of Reynolds numbers are low in our studied configurations ($Re_V < 200$) and thus the vapour flow is laminar.

Final heat flux expression

To conclude, knowing $R_s(t)$, t_R and $\delta_V(t)$, the final expression of the heat exchanged between the hot surface and the droplet is given by equation 17 :

$$\Phi = \pi\Big[\frac{8}{9}(Nu\ \lambda_V (T_W - T_{SAT}) R_d)^3 \frac{\rho_V \rho_L h^*_{LV}[g + a_n]}{\mu_V}\Big]^{1/4} \int_0^{t_R} R_s(t)dt + \epsilon_w \sigma_B (T_W^4 - T_L^4)\pi \int_0^{t_R} R_s^2(t)dt \tag{17}$$

Results and Discussion

In this section, the elaborated model will first be discussed against an experimental case and finally the comparaison to the whole data is given.

Results and assumptions validation

The chosen case is $D_d = 145\mu m$, $V_n = 4m/s$ thus $We = 30$. The evolutions of the experimental and analytical (eq. 8) spreading diameters as well as of the vapour thickness are displayed in figure 8.

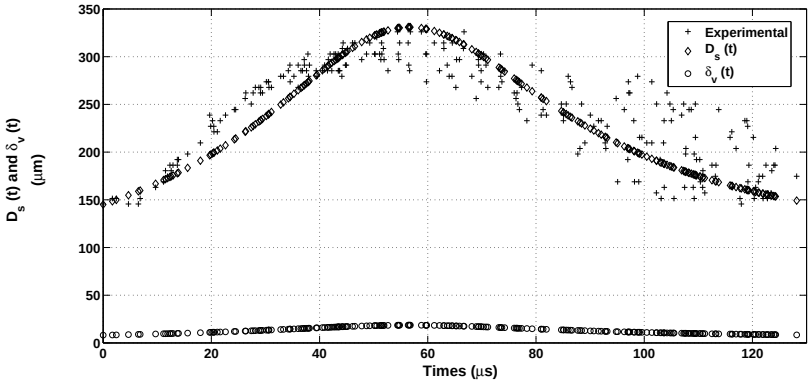

Figure 8. Evolution of the spread diameter and vapour cushion thickness versus time ($D_d = 145\mu m$, $V_n = 4m/s$, $T_W = 600^oC$)

The experimental variation of the diameter of the flattened part of the droplet surface during the bounce is well reproduced. Also, from this figure, one can notice that, whereas the droplet diameter varies from $145\mu m$ to $330\mu m$ (about a factor of two), the vapour thickness varies from $7\mu m$ to $16\mu m$. Thus, as the droplet spreading diameter is one order of magnitude larger than the vapour thickness, this validates the previous assumption that the vapour normal velocity is negligible.

Moreover, as observed in figure 8, the vapour thickness slightly increases during the bounce. This comes from the relation 16 between the spread diameter and this thickness. Indeed, vapour mass flow rate beneath this flattened surface increases with this surface and consequently, by flow rate conservation, the section of the vapour interlayer flow rises. These results are consistent with numerical results from literature [17], [18] and [19] where vapour thicknesses of the same order of magnitude (tens of μm under droplet of hundered of μm) are reported and where this thickness also rises during the droplet bounce in Leidenfrost regime.

In these conditions ($D_d = 145\mu m$, $V_n = 4m/s$), it is also possible to evaluate from equation 17 the convective and radiative parts of the exchanged heat flux. The convective part is $0.1mJ$ whereas the radiative part is $1.05\ 10^{-4}mJ$ which is thus negligible. This observation, done in this particular case, could be extended to all our studied cases where the droplet diameters and velocities are very small.

However, the spread diameter evolution is not the characteristic parameter of our present model. This parameter is rather $\int_0^{t_R} R_s(t)dt$ as it appears in the first term of the right hand side of the final expression (eq. 17) (the second being negligible) . We have compared this integral to our 52 experimental data and found a low relative average error of 7%. This error is related to the evaluation of $R_s(t)$ through the spring analogy but also to the evaluation of t_R using the Biance's model. It has been shown that an uncertainty of 10 % on t_R leads to about an error of 5% on $\int_0^{t_R} R_s(t)dt$.

To complete the discussion on this particular case results, the heat exchange effectiveness is $\epsilon = 0.0227$. More generally, the effectivnesses got from our experimental tests are one order of magnitude more important than the ones observed by Kendall [7] and Ueda [8] for similar conditions. However, this liquid loss corresponds to relative variations of the droplet diameter less than 1 %. This validates the consideration of the volume balance equation 7.

Heat flux evolution

Figure 9.a presents the energy lost by the wall and caused by the impact of a droplet of diameter $D_d = 250\mu m$ and normal velocity $V_n = 2.7m/s$. The injector frequency is ajusted such as there is no collision of droplets onto the surface and that each of droplet produces an independent effect on the heat removal [11]. The vapour layer insulated the droplets and limits considerably the experimental heat exchanged between the droplet and the surface ($\Phi \sim 0.5mJ$). In the remaining part of this process, the slab is cooled below the Leidenfrost temperature and the droplets, entering in contact with the slab, creates a liquid film. This boiling film increases the heat removal ($\Phi > 4.5mJ$). The heat derived from the model (eq. 17) is also plotted in figure 9.a. The experimental heat slightly decreases with the wall temperature with quite the same slope as the heat derived from our model. The physical behaviour occuring below the Leidenfrost temperature is not reproduced in our model. That is why the model gives not the observed rise of heat exchanged. The dependence of the modelled heat exchange on the wall temperature seems thus to be consistent. As shown in figure 9.b, it is a little bit lower but is of the same order of magnitude as the experimental heat on the contrary to the heat evaluated from Guo's correlation (eq. 1 - $\sim 0.05mJ$).

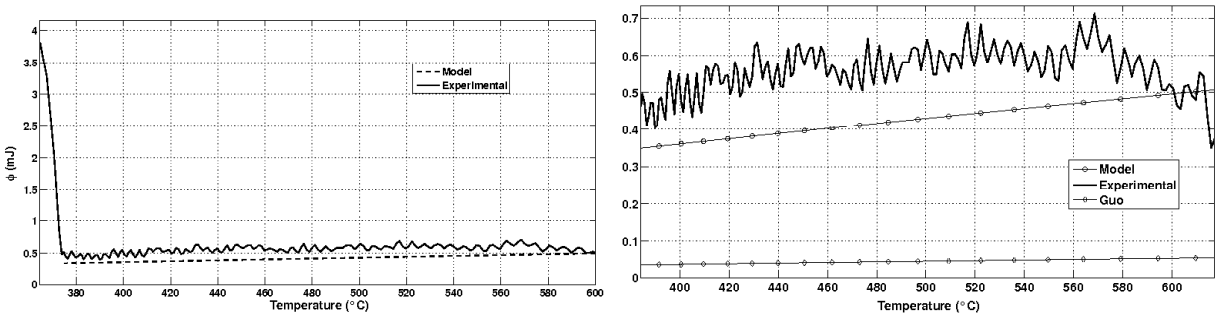

Figure 9. Evolution experimental and calculated heat fluxes versus temperature ($D_d = 250\mu m$, $V_n = 2.7m/s$)

More global results

Finally, heat exchanges evaluated through equation 17 are compared to data obtained for water droplets streams for different diameters and velocities. In figure 10 and 11 the calculated evolutions of heat removal obtained for droplets velocity $V_n = 2.5m/s$ and $V_n = 3m/s$ are compared to experimental heat evolutions obtained considering the same droplets streams ($D_d = 130, 160$ and $250\ \mu m$). From these figures, one is aware of the difficulty to measure such very low heat fluxes. The heat removals undergo large variations compared to their low average values. This experimental issue is widely discussed in [11] especially the role of the noise in the measurement. This noise is at the origin of the measured negative heat fluxes in particular for the smallest droplet diameters $D_d = 130\ \mu m$. Nevertheless the heat dependency on the droplets diameter is quite well reproduced. The order of magnitude of the heat exchange is correct. There also is a good agreement between the correlation 17 and the data whatever the velocity is.

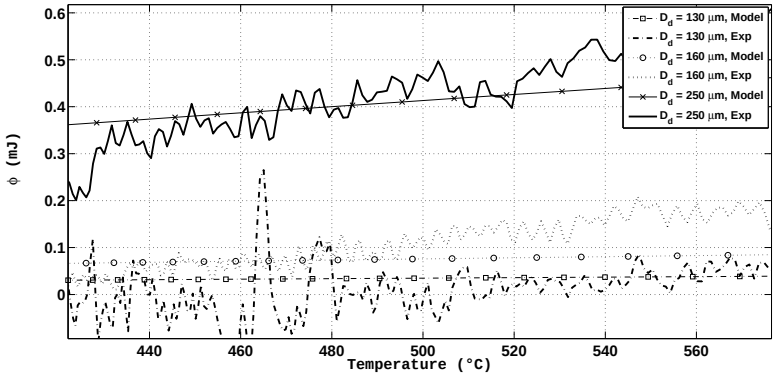

Figure 10. Evolution experimental and calculated heat exchanges versus temperature ($V_n = 2.5m/s$)

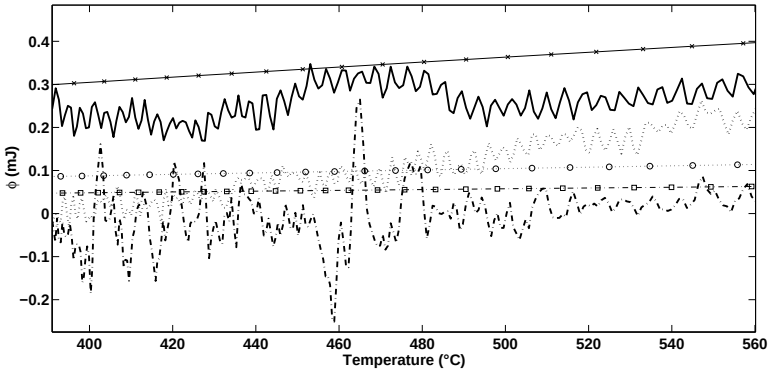

Figure 11. Evolution experimental and calculated heat exchanges versus temperature ($V_n = 3m/s$)

Conclusion

This study is carried out within the framework of the evaluation of the coolability of damaged PWR reactor assemblies in the core during a Loss Of Coolant Accident. During the reflooding phase of such an accident, core cooling is first provided by a mist flow of superheated vapour carrying subcooled small water droplets which impact the swollen fuel cladding. This cladding is well above the Leidenfrost temperature and the droplets experience perfect bouncing impact regime. Although this issue is highly relevant for the nuclear reactor safety and that many experimental studies exist on the dynamics of droplets impacting onto a hot surface, very few studies focus on the heat exchange between the droplet and the wall in the bouncing regime. That is why, a new experimental set-up, designed to measure the cooling flux in the LOCA conditions (low Weber numbers ; low droplet diameter and velocity of few m/s), was performed at the LEMTA.

The experimental heat fluxes are recorded once the heating of the surface stops. The heat exchanged in the Leidenfrost regime are quite low (few mJ per droplet impact). Indeed, when the droplet reaches the hot wall, it flattens out on a thin vapour layer generated beneath the droplet and insulating the liquid from the wall. As only a very small part of the droplet evaporates during its rebound, the dynamical and thermal approaches of this issue have been separately treated. An expression of the heat exchanged have been fulfilled determined from, on the one hand, a dynamical spring analogy which provides the evolution of the spreading diameter of the droplet (the flattened surface in front of the heated wall), and on the other hand, a thermal balance in the vapour interlayer which gives the vapour thickness. The assumptions have been validated on an experimental case and extended to all the LOCA conditions. It has finally been shown that the exchanged heat flux is mainly a convective heat flux throughout vapour thickness and leads to the evaporation of a tiny part of the droplet.

Finally, the evolution of the spreading diameters and of the exchanged heat fluxes have successfully been validated against experimental data. The results have also been compared to heat exchange expressions from the literature. It has been found that the heat flux of Guo [9] largely under estimates the data and the heat exchange effectiveness given by Kendall [7] and Ueda [8] also are one order of magnitude below our experimental results.

Numerous experimental runs are currently performed in order to generate an important data base on horizontal and inclined Nickel and Zircaloy slabs which are more representative of nuclear cladding. Also an evaluation of experimental uncertainty is underway.

Nomenclature

a	acceleration $[m/s^2]$	*Greek Letters*	
C_p	specific heat $[J/kg/K]$	δ	vapour thickness $[m]$
D	diameter $[m]$	ϵ	effectiveness $[-]$
E	energy $[J]$	ϵ_B	Stephan-Boltzmann's constant $[W/m^2/K^4]$
G	flow rate$[kg/m^2/s]$	ϵ_w	wall emissivity $[-]$
g	gravity $[m/s^2]$	η	damping coefficient $[kg/s]$
h_{LV}	Latent heat $[J/kg]$	λ_V	vapour thermal conductivity $[W/m^2/K]$
k	stiffness $[kg/s^2]$	μ	dynamic viscosity $[kg/m/s]$
m	mass $[kg]$	ρ	density $[kg/m^3]$
Nu	Nusselt number $[-]$	σ	surface tension $[kg/s^2]$
P	pressure $[Pa]$	ω	pulsation $[s^{-1}]$
R	radius $[m]$	Φ	heat Flux $[J]$
Re	Reynolds number $[-]$		
S	surface $[m^2]$	*Subscript*	
t	time $[s]$	d	Droplet
t_R	resident time $[s]$	DC	Direct Contact
T	temperature $[K]$	L	Liquid
u	vapour velocity $[m/s]$	SAT	Saturation
V	droplet velocity $[m/s]$	V	Vapour
Y	point mass location $[m]$	W	Wall
We	Weber number $[-]$		

References

[1] Peake, W.T., *Dispersed flow film boiling during reflooding*, PhD Thesis, University of California, Berkley (1979).

[2] Wong, S., Hochreiter, L.E., A model for dispersed flow heat tranfer during reflood, *19th Nation,al Heat Tranfer Conference* (1980).

[3] Lee,R. , Reye, J.N., Almenas,K. , Size and number density change of droplet populations above a quench front during reflood, *Int. J. Heat and Mass Transfer* , 27 (4):573-585 (1984).

[4] Leidenfrost, J.G., On the fixation of water in diverse fire, *Int. J. Heat and Mass Transfer* 9, 1153-1166 (1966).

[5] Wachters, L.M.J., Westerling, N.A.J., The heat transfer from a hot wall to impinging water drops in the spheroidal state, *Chem. Eng. Science* , 21 :1047-1056 (1966).

[6] Karl, A., Frohn, A., Experimental investigation of interaction processes between droplets and hot walls, *Physics of fluids*, 785 (2000).

[7] Kendall G.E., heat transfer to impacting drops and post critical heat flux dispersed flow. PhD thesis, Dept. Mechanical Engineering (1978).

[8] Ueda, T., Enomoto, T., Kanetsuki, M., Heat transfer characteristic and dynamic behaviour of saturated droplets impinging on a heated vertical surface, *B*ulletin of the JSME (1979).

[9] Guo, Y., Mishima, K,. A non equilibrium mechanistic heat transfer model for post-dryout dispersed flow regime, *Exp. Thermal and Fluid Science*, 26, 861-869 (2002).

[10] Biance A. L., Chevy F. , Clanet C., Lagudeau G., Quere D., On the elasticity of an inertial liquid shock, *J. Fluid. Mech* ., 554, 47-66 (2006).

[11] Lelong, F., Gradeck, M., Rémy, B., Ouattara, A., Maillet, D., Inverse Conduction Technique in Hankel domain using infrared thermography: Application to droplet stream quenching a metal disk, *IHTC14*, Washington, August 2010.

[12] Lelong, F., Gradeck, M., Maillet, D., Seiler, N., Experimental study of heat transfer between droplets and wall in Leidenfrost regime, 7th *Int. Conference on Multiphase Flow (ICMF)*, Tampa, FL USA, May 30-June 4, 2010.

[13] Castanet, G., Liénart, T., Lemoine, F., Dynamics and temperature of droplets impacting onto a heated wall, *Int. J. of Heat and Mass Transfer* 52:670-679 (2009).

[14] Bolle, L., Moureau, J.C., Spary cooling of hot surface, G.F Hewitt, J.M. Delhaye, N. Zuber (Eds), *Multiphase*

Science and Technology, vol.1, Hemisphere Publishing, Washington, DC, 1982.
[15] Buyevich, YU. A., Mankevich, V.N., Interaction of dilute mist flow with a hot body, *Int. J. Heat and Mass Transfer*, 38 (4): 731-744 (1995).
[16] Incropera, F. P., DeWitt, D.P., Fundamentals of Heat and Mass Transfer, *J. Wiley and Sons*, (2006).
[17] Chatzikyriakou, D., Walker, S.P., Hewitt, D.F., Narayanan, C., Lakehal, D., Comparison of measured and modelled droplet-hot wall interaction, *Applied Thermal Engineering*, 29 (7):1398-1405 (2008).
[18] Ge, Y., Fan. L.S., Three-dimensional simulation of impingement of a liquid droplet on a flat surface in the Leidenfrost regime, *Physics of Fluids*, 17, 027104 (2005).
[19] Zhao, Y., Yang, G. Fran, L.S., Multi-scale simulation of oblique collision of a droplet on a surface in the Leidenfrost regime, *Chemical Engineering Science*, 62:3462-3472 (2007).